Atmos. Meas. Tech. Discuss., 7, 1027–1057, 2014
www.atmos-meas-tech-discuss.net/7/1027/2014/
doi:10.5194/amtd-7-1027-2014

Atmospheric Measurement Techniques Discussions

A high-resolution oxygen A-band spectrometer (HABS) and its radiation closure

Q. Min[1], B. Yin[1], S. Li[1], J. Berndt[1], L. Harrison[1], E. Joseph[1], M. Duan[2], and P. Kiedron[3]

[1]Atmospheric Science Research Center, State University of New York, Albany, NY 12203, USA
[2]LAGEO, Institute of Atmospheric Physics, Chinese Academy of Sciences, Beijing, China
[3]Cooperative Institute for Research in Environmental Sciences, University of Colorado, Boulder, Colorado, USA

Received: 17 January 2014 – Accepted: 23 January 2014 – Published: 5 February 2014

Correspondence to: Q. Min (qmin@albany.edu)

Published by Copernicus Publications on behalf of the European Geosciences Union.

Abstract

The pressure dependence of oxygen A-band absorption enables the retrieval of the vertical profiles of aerosol and cloud properties from oxygen A-band spectrometry. To improve the understanding of oxygen A-band inversions and utility, we developed a high-resolution oxygen A-band spectrometer (HABS), and deployed it at Howard University Beltsville site during the NASA Discover Air-Quality Field Campaign in July 2011. The HABS has the ability to measure solar direct-beam and zenith diffuse radiation through a telescope automatically. It exhibits excellent performance: stable spectral response ratio, high signal-to-noise ratio (SNR), high spectrum resolution (0.16 nm), and high Out-of-Band Rejection (10^{-5}). To evaluate the spectra performance of HABS, a HABS simulator has been developed by combing the discrete ordinates radiative transfer (DISORT) code with the High Resolution Transmission (HTRAN) database HITRAN2008. The simulator uses double-k approach to reduce the computational cost. The HABS measured spectra are consistent with the related simulated spectra. For direct-beam spectra, the confidence intervals (95 %) of relative difference between measurements and simulation are (−0.06, 0.05) and (−0.08, 0.09) for solar zenith angles of 27° and 72°, respectively. The main differences between them occur at or near the strong oxygen absorption line centers. They are mainly caused by the noise/spikes of HABS measured spectra, as a result of combined effects of weak signal, low SNR, and errors in wavelength registration and absorption line parameters. The high-resolution oxygen A-band measurements from HABS can constrain the active radar retrievals for more accurate cloud optical properties, particularly for multi-layer clouds and for mixed-phase clouds.

AMTD
7, 1027–1057, 2014

1 Introduction

Oxygen A-band (759–770 nm) is one of the most prominent near-infrared features in the atmosphere. It has been studied extensively for remote sensing from satellite measurements to ground-based measurements (Grechko et al., 1973; Mitchell and O'Brien, 1987; Fischer and Grassl, 1991; Fischer et al., 1991; O'Brien and Mitchell, 1992; Harrison and Min, 1997; Pfeilsticker et al., 1998; Veitel et al., 1998; Min and Harrison, 1999, 2004; Portmann et al., 2001; Min et al., 2001, 2004c; Min and Clothiaux, 2003; Li and Min, 2011, 2013). Oxygen is a well-mixed gas in the atmosphere; the pressure dependence of oxygen A-band absorption line parameters provides a practical way for retrieving photon path length distributions and vertical information of aerosols and clouds (Harrison and Min, 1997; Pfeisticker et al., 1998; Veitel et al., 1998; Min and Harrison, 1999, 2004; Portmann et al., 2001; Min et al., 2004c; etc.). However, routine measurements of oxygen A-band spectra are from low- or moderate-resolution spectrometers. As discussed in Min and Clothiaux (2003), the low- or moderate-resolution oxygen A-band spectra only can provide two independent retrieved parameters of photon path length distribution.

In principle, high-resolution oxygen A-band spectra can discriminate atmospheric scattering from surface scattering, and thus provide a better remote sensing technique to retrieve cloud and aerosol macrophysical/microphysical properties (Stephens and Heidinger, 2000; Heidinger and Stephens, 2000, 2002; Min and Harrison, 2004; Stephens et al., 2005). As stated in Min and Harrison (2004), with high-resolution oxygen A-band measurements, four or five independent pieces of information can be obtained, depending on the instrument resolution, the Out-Of-Band (OOB) rejection, and the Signal-to-Noise Ratio (SNR).

To understand oxygen A-band inversions and utility, we developed a high-resolution oxygen A-band spectrometer (HABS) with polarization capability. It was deployed at Howard University Beltsville Campus (HUBC) in Maryland during the NASA Discover Air-Quality Field Campaign in July 2011. This paper specifically reports on the

AMTD
7, 1027–1057, 2014

development of the HABS and its spectral performance. We evaluate the spectral performance of HABS through radiation closure by comparing HABS measured spectra with simulated spectra. The simulation of high-resolution oxygen A-band spectrum is based on our HABS simulator that combines the discrete ordinates radiative transfer (DISORT) model (Stamnes et al., 1988) with the High Resolution Transmission (HTRAN) database HITRAN2008 (Rothman et al., 2009). More importantly, all key model inputs are based on the collocated measurements during the field campaign. In particular, aerosol optical properties are derived from a Multi-Filter Rotating Shadowband Radiometer (MFRSR) and a Raman Lidar. MFRSR provides measurements of spectral solar radiation and retrieved aerosol and cloud optical properties (Min and Harrison, 1996; Min et al., 2003, 2004a, b, 2008). Raman Lidar has the ability to measure the vertical profiles of aerosol scattering ratio at high time resolution and height resolution (Connell et al., 2009). Further, we discuss the potential applications of HABS spectra measurements.

2 Instrument design and its performance

2.1 Instrument design

The HABS, shown in Fig. 1, was developed by the Atmospheric Science Research Center (ASRC) of State University of New York at Albany. It consists of an alt-azimuth tracker fore-optics, a high-resolution grating monochrometer, a high performance charge-coupled device (CCD) assembly, and a temperature controlling system.

A sketch of the HABS optics is shown in Fig. 2. Through a telescope with a field of view (FOV) of 2.71° and a pair of total reflection prisms, the alt-azimuth tracker can track the sun or point to the zenithal direction automatically. This fore-optic enables to measure both direct beam and diffuse radiances using the same system. Since the photon path length distribution is known for direct beam radiance (e.g., a δ function), the direct beam measurements can be used to assess instrument functions and absorption line

AMTD
7, 1027–1057, 2014

parameters with simple Beer's law. As demonstrated by Min and Clothiaux (2003), the direct beam measurements can be also used to construct the retrieval kernels directly. The well-tested instrument functions and line parameters or the constructed retrieval kernels from direct beam measurements are readily used for the retrievals from diffuse radiance measurements.

The grating monochrometer consists of a high line-density grating (1800 grooves per mm) and two long focal-length mirrors with focal lengths of 32 inches and 38 inches. It provides high-resolution spectrally-resolved direct-beam and zenith diffuse radiance on a CCD array (256 × 1024), covering the entire oxygen A-band from 759 nm to 769 nm. The spectrometer was equipped with a high performance CCD camera. The CCD area of the system is thermoelectrically cooled to −70 °C to reduce the readout noise. The whole optical system is housed in an enclosure to maintain temperature stability and to protect it from the weather. As a high-resolution spectrometer, the instrument is sensitive to the environment temperature, which can result in the spectrum wavelength shifting (Li and Min, 2012). Because each pixel measures different portions of absorption spectrum, the spectrum shifting will bring in errors to the retrieval processes. To alleviate these errors, a temperature controlling system was implemented into the instrument, which consists of a temperature controller, temperature sensors, fans, heaters, and a water cooling subsystem (not shown here). This temperature controlling system can keep the HABS inner temperature stable within 0.1 °C. It helps to restrain the spectrum shifting and protect the instrument components from outside temperature variations.

In the fore-optic module of HABS, two filters are used to suppress radiation outside the band, and an electronic shutter is used to control the time of exposure. A filter wheel in the fore-optic enables six modes: open mode, diffuser mode, and four polarizer modes with different orientations (i.e., 0°, 45°, 90°, and 135°), as shown in Fig. 2. The diffuser mode is used for direct-beam measurements, to reduce signal and fill up the slit of the spectrograph. The open mode and four polarizer modes are used for zenith diffuse measurements. The polarizer modes enable to measure the degree of polarization

AMTD
7, 1027–1057, 2014

in the atmosphere, which enhance retrieval capability of oxygen A-band spectroscopy. Also, the grating and mirrors are polarization-dependent reflectivity properties. Neglect of such an instrument's polarization sensitivity can lead to errors of several tens of percent in the values of radiance measured at wavelengths where the instrument's polarization sensitivity is highest (Natraj et al., 2007; Stam, 2005; Levy et al., 2004; Schutgens and Stammes, 2003; Oikarinen, 2001; Lacis, 1998; Mishchenko et al., 1994; Charles et al., 1994).

The four polarizer modes can be used to derive the degree of polarization (DOP) for the oxygen A-band spectra, through Eqs. (1–5) (Berry et al., 1977; McMaster, 1954, 1961).

$$I = I(0°) + I(90°) = \langle |E_x|^2 + |E_y|^2 \rangle \quad (1)$$

$$Q = I(0°) - I(90°) = \langle |E_x|^2 - |E_y|^2 \rangle \quad (2)$$

$$U = I(45°) - I(135°) = \mathrm{Re}\langle E_x E_y \rangle \quad (3)$$

$$V = 0 = \mathrm{Im}\langle E_x E_y \rangle \quad (4)$$

$$\mathrm{DOP} = (Q^2 + U^2 + V^2)^{1/2} / I \quad (5)$$

where we choose a Cartesian coordinate system (x, y, z) to indicate the light propagation. E_x and E_y are the electric field components in the x and y directions, perpendicular to the direction of light propagation z. $I(0°)$, $I(45°)$, $I(90°)$, and $I(135°)$ are HABS measured polarized radiances under different polarization modes. I, Q, U, and V are the four Stokes parameters; and DOP is the derived degree of polarization. The measurement of polarization of oxygen A-band spectra improves the retrieval ability for aerosols and ice clouds.

2.2 Instrument performance

As stated previously, before the incident light arrives at the entrance slit of grating spectrometer, it passes through a pair of prisms, two bandpass filters, and one of the filter

AMTD
7, 1027–1057, 2014

wheel channels. This will modulate the spectrum shape of the incident light, which can be presented by "filter function". To calibrate the response of the overall filter function, we use the lamp GS0937. The spectrum response ratios at different channels of filter wheel are shown in Fig. 3. They are indicated by the ratios of the spectra after using the filters and the spectra before using the filters. These response functions changed very little during long-term in-lab experiments and field observations, suggesting very stable performance of the HABS.

As discussed in Min and Harrison (2004), the slit function is crucial for evaluation of spectrometer performances. The slit function of the HABS was once obtained using an Ar Lamp (763.511 nm) and used for wavelength registration study (Li and Min, 2012). However, some contamination of other weak emission lines of the Ar lamp may contribute to the stray light of the slit function. In this study, we used a laser diode DFB-763 (763.0 nm) to measure the slit function. As shown in Fig. 4, the Full Width at Half Maximum (FWHM) is about 1.55 pixels or 0.016 nm (about 0.26 cm^{-1} at oxygen A-band), which is narrower than the Ar Lamp measured one (i.e.,1.85 pixels or 0.019 nm or 0.30 cm^{-1}). The OOB rejection is about 10^{-5}, similar to the Ar lamp measurement.

The SNR is determined by both readout and Poisson noise terms. When the signal is weak, such as the signal near an absorption line center, the readout noise (and Poisson noise of dark signal) dominate(s). Due to the low temperature (about −70 °C) of the CCD module, the Standard Deviation (SD) of readout noise for CCD pixels is less than 5 counts, and their mean value is about 3 counts. Figure 5 shows one case of the SNR. It is estimated based on 24 consecutive measurements, in which each exposure is 0.25 s. The minimum SNR is 78 and 111 in *R* and *P* branches, respectively. The signal strength depends on solar zenith angle and sky conditions, so does the SNR. To obtain the best SNR, the exposure time is automatically adjusted based on the strength of incident solar radiation.

In this spectrometer the FWHM of the instrument function is 0.016 nm, thus measurements of sharply-structured absorption features are very sensitive to small spectral shifts. For HABS, the impact of wavelength shift has been extensively discussed

AMTD
7, 1027–1057, 2014

by Li and Min (2012). Even if a very small wavelength shift (e.g., 0.001 nm) occurs, the distribution of oxygen absorption optical depth contributing to the absorption line center will change significantly. To reduce the error induced by the wavelength shift, Li and Min (2012) developed a self-calibrating wavelength registration method. This method can accurately register each measured spectrum individually and fast. In this study, we used this method to make wavelength registration.

2.3 HABS measurements

We deployed the HABS at HUBC during the NASA Discover Air-Quality Field Campaign in July 2011. During this field campaign, many instruments (e.g., MFRSR, Raman Lidar, sonde balloon, etc.) worked together to observe the air-quality, aerosol and cloud properties.

Figure 6a shows HABS measured oxygen A-band direct beam spectra and the related zenith diffuse spectra under clear day situations. Figure 6b shows two HABS measured oxygen A-band zenith diffuse spectra for thick clouds and cirrus clouds, respectively. It is clear that the absorption lines are individually resolved and they have very large dynamic range. This indicates that the HABS measured oxygen A-band spectra have the capability to retrieve the photon path length and thus retrieve the vertical profiles of cloud.

Figure 7 shows one case of the measured high-resolution oxygen A-band spectra of zenith diffuse radiation for four polarizations. It was measured at 13:08 (GMT) on 26 July 2011. In this case, no cloud exists; solar zenith angle (SZA) is 56°, and the MFRSR derived AOD (at 760 nm) is about 0.04. Obviously, the spectra measured under polarization modes are smaller than under the open mode and vary significantly with polarizer orientations. The derived DOP spectrum, shown in Fig. 7b, exhibits polarization characteristics associated with oxygen absorption lines. As shown in Eqs. (1)–(5), DOP is derived through subtractions among four spectra. The residuals are extremely sensitive to the signal-to-noise ratio (SNR) of spectrometer. Weak signals and low SNRs at the strong absorption line centers could result in some noise

AMTD
7, 1027–1057, 2014

in the DOP spectrum. Additionally, slight shifts of wavelength associated with different spectra could also result in spikes in the DOP spectrum. Again, those spikes are at or near the strong absorption line centers, as a result of the combined effect of weak signals, low SNRs, and slight wavelength shifts. The issues about HABS polarization measurements will be evaluated and analyzed in detail in another paper about the HABS in the near future.

3 Simulation of high-resolution oxygen A-band spectra

Analyzing the high-resolution spectra measurements and applying them to the retrievals of cloud and aerosol properties require forward radiative transfer calculations to simulate the observed spectra. For the measured spectra, each pixel contains spectral response of multiple absorption lines, convolving with the slit function. Therefore, to simulate a high-resolution measured spectrum, we need to make radiative transfer calculations at much higher spectral resolution in a line-by-line domain. However, running a radiative transfer model in a line-by-line domain is very time-consuming. To reduce the computational cost for operational retrievals, Duan et al. (2005) developed a fast radiative transfer model by using a double-k distribution approach. Based on this fast radiative transfer model, we developed a HABS simulator to simulate the HABS measurement.

3.1 Calculation of oxygen absorption optical depth profiles

To simulate the oxygen A-band spectra at high spectral resolution, vertical profiles of oxygen absorption optical depth are required in a line-by-line domain. In this study, the oxygen absorption profiles are originally calculated by the Line-By-Line Radiative Transfer Model (LBLRTM 12.1) (Clough et al., 2005) based on the HTRAN database HITRAN2008. However, calculating oxygen absorption optical depth profiles with LBLRTM is also very time-consuming (more than 5 h for the entire oxygen A-band

AMTD
7, 1027–1057, 2014

by a fast PC). Because the atmospheric structure is always changing with time, frequent recalculation of the oxygen absorption optical depth profiles is required. To reduce the computational cost, it is necessary to develop a fast method to recalculate the oxygen absorption optical depth profiles accurately.

As stated previously, the oxygen absorption coefficients are determined by the atmosphere pressure and temperature. Chou and Kouvaris (1986) proposed that the absorption coefficients (k) at wavenumber (v) can be defined as a function of air pressure (p) and temperature (T) as shown in Eq. (6).

$$\ln(k(v,p,T)) = a_0(v,p) + a_1(v,p)\cdot(T - T_{\text{mean}}) + a_2(v,p)\cdot(T - T_{\text{mean}})^2 \quad (6)$$

where, a_0, a_1, a_2, and T_{mean} are previously calculated parameters by fitting three pairs of given (p,T). In a similar way, the oxygen absorption optical depth (τ) can be also defined as a function of p and T for any atmospheric layer as shown in Eq. (7).

$$\ln(\tau(v,p,T)) = a_0(v,p) + a_1(v,p)\cdot(T - T_{\text{mean}}) + a_2(v,p)\cdot(T - T_{\text{mean}})^2 \quad (7)$$

In this study, all parameters of Eq. (7), i.e., a_0, a_1, a_2, and T_{mean}, are derived by the results of three or more given atmospheric profiles. In the LBLRTM model, there are six typical geographic-seasonal model atmospheres, i.e., tropical model, mid-latitude summer model, mid-latitude winter model, subarctic summer model, subarctic winter model, and Unites States Standard (1976) model. Based on these six model atmospheres, six sets of oxygen absorption optical depth profiles are calculated in the line-by-line domain. Using three of them, we derive the three parameters (i.e., a_0, a_1, a_2) in Eq. (7) for every wavenumber. These derived parameters are stored in a parameter database in the line-by-line domain. The oxygen absorption optical depth profiles for all the six model atmospheres have been recalculated through Eq. (7) with derived parameters and compared with the original LBLRTM calculations. The comparison indicates that the accuracy of the fast parameterization scheme is within 1 % (not shown here) and the computing time is reduced to 0.2 %

AMTD
7, 1027–1057, 2014

3.2 Double-*k* distribution approach

Based on the calculated oxygen absorption optical depth profiles and other observed or derived atmospheric properties (e.g., surface albedo, solar zenith angle, and etc.), we use the DISORT to calculate radiative transfer in the atmosphere. Although the LBLRTM model can be used to simulate the super high spectra resolution radiance, it is very time consuming. A fast and accurate forward radiative transfer model is crucial to reduce the computational cost for operational retrievals. Min and Harrison (2004) outlined a k-distribution approach for simulating the oxygen A-band spectrum under clear-sky conditions. In their approach, the radiation from absorption and scattering processes of cloud and aerosol is split into the single- and multiple-scattering components: the first scattering component is computed accurately, and multiple scattering (second order and higher) radiance is calculated approximately. Duan et al. (2005) extended and modified this technique to all-sky conditions on the basis of the equivalent theorem with a double-*k* distribution approach to account for the uncorrelated nature of overlapped absorption lines. In this double-*k* approach, two integrated absorption optical depths, the total absorption optical depth, k, and absorption optical depth from the top of the atmosphere to the scattering layer, k_0, are used to account for the vertical distribution of gaseous absorption in multiple-scattering media. In this study, we use the DISORT code coupled with the double-*k* distribution approach to simulate the oxygen A-band spectrum.

3.3 HABS fitting model

To simulate the HABS measurements, the model calculated super high-resolution spectrum needs to be convolved with the instrument slit-function. As stated previously, the measured HABS slit function shows very good local monochromatic property. However, its spectral resolution is much lower than the required spectral resolution of the forward model. To match the model calculated spectra, we interpolate the measured HABS slit-function to the model resolution. At the peak center of slit-function, the choice

AMTD
7, 1027–1057, 2014

of interpolating function has substantial impacts on the shape of the slit-function (Li and Min, 2012). In this study, we used the same method as Li and Min (2012), which has been proven to have the ability to make an accurate fitting calculation.

4 Comparison of HABS measurements with model simulations

As shown in Fig. 8a, MFRSR measurements indicate that 26 July 2011 was a good clear day for radiation closure study of HABS. The vertical profiles of air pressure and temperature on that day were provided by the collocated sonde balloon measurements (shown in Fig. 9a and b). In the model simulation, to be consistent with the oxygen absorption optical depth profiles, the sonde balloon measured profiles are layered into 34 atmospheric layers, with an increment of air pressure of 30 mbar. The aerosol extinction coefficients profile (shown in Fig. 9c), is estimated from Raman Lidar measured aerosol scattering ratio profile, for which the total extinction is normalized by the MFRSR measured aerosol optical depth (shown in Fig. 8b).

The comparisons of measured and simulated direct-beam spectra at the oxygen A-band under different solar zenith angles (SZA) are shown in Fig. 10. The difference of normalized radiance between observation and simulation is very small. The maximum relative difference between them often occurs at or near strong absorption line centers, which is very sensitive to wavelength shift and has low SNR (Fig. 7b). At small SZA (e.g., SZA = 27°), the confidence interval (95 %) of relative difference is (−0.06, 0.05). At large SZA (e.g., SZA = 72°), the SNR at or near strong absorption line centers decreases significantly. The confidence interval of relative difference is (−0.08, 0.09). Figure 11 shows the comparisons of normalized direct-beam radiance of the oxygen A-band spectra vs. air mass. In this study, the normalized radiances at five wavelengths are chosen for analysis (shown in Fig. 11b). In general, the HABS direct-beam measurements and model simulations are basically consistent with each other at different air masses. Meanwhile, for any given wavelength position, the logarithmic values of normalized radiance decreases quasi-linearly with air mass. The slight non-linear part

AMTD
7, 1027–1057, 2014

is caused by strong oxygen absorption and by temporal variation of atmospheric profiles (e.g., temperature profile, pressure profile, and aerosol profile).

Figure 12 shows the comparisons of measured and simulated zenith diffuse spectra at the oxygen A-band for different SZAs. The measured zenith diffuse spectra used for comparison are combined by the measurements from 4 polarizer channels (e.g., $I(0^\circ) + I(90^\circ)$ or $I(45^\circ) + I(135^\circ)$). The combined measured spectra have the ability to remove or constrain the impacts of the instrument polarization performance. The difference of normalized radiance between observation and simulation is also quite small. The relative difference of diffuse spectra between observation and simulation is similar to that of direct-beam spectra. With SZA of 27° and 72°, the confidence intervals of relative differences are (−0.06, 0.05) and (−0.08, 0.07), respectively. In particular, in the wavelength range around the strong oxygen absorption line centers (e.g., range of 763 nm to 765 nm), we found that the simulated value at the absorption line centers tends to be slightly smaller than observation. This could be caused by two factors: (1) the error of instrument slit function measurement and oxygen absorption line parameters; and (2) Raman scattering effects. The Raman scattering will slightly compensate the absorption in the strong absorption ranges, which currently cannot be simulated by the HABS simulator. In general, the HABS observation and the related model simulation of zenith diffuse radiance at the oxygen A-band are basically consistent with each other. Certainly, further assessments of instrument slit function and performance, oxygen absorption line parameters, and Raman scattering effect are warranted.

5 Summary

The newly developed high-resolution A-band spectrometer (HABS) was evaluated with in-lab tests and through a deployment during the NASA Discover-AQ field campaign at HUBC in July 2011. The HABS exhibits excellent performance: stable spectral response ratio, high SNR of 100 at the darkest pixels in the *P* branch, high spectrum resolution of 0.16 nm or 0.26 cm^{-1}, and high Out-of-Band Rejection of 10^{-5}. With such

AMTD
7, 1027–1057, 2014

specifications, the HABS measured oxygen A-band spectra is able to derive at least four independent pieces of information (Min and Harrison, 2004). With an alt-azimuth tracker fore-optics, the HABS measures both direct beam and diffuse radiances with the same system, enabling better assessments of instrument functions and absorption line parameters and construction of retrieval kernel functions (Min and Clothiaux, 2003). More importantly, the HABS has the capability to measure the polarization of atmospheric scattering, providing additional information for scattering particle shapes.

The HABS spectra measurements and model simulations are basically consistent with each other. The significant/large relative differences between them mainly occur at or near the strong absorption line centers, which increase with the SZA. For the direct-beam spectra, the confidence intervals (95 %) of relative difference between measurements and simulations are (−0.06, 0.05) and (−0.08, 0.09) for SZAs of 27° and 72°, respectively. For the zenith diffuse spectra, the confidence intervals of relative difference are (−0.06, 0.05) and (−0.08, 0.07) for SZAs of 27° and 72°, respectively. In particular, at big SZAs, the simulated zenith diffuse radiance at the absorption line centers tends to be slightly smaller than observed one. This could be caused by Raman scattering effects.

This HABS provides accurate radiance and polarization spectra of both direct beam and zenith diffuse for evaluation and validation and for retrievals of photon path length distribution and vertical properties of aerosols and clouds (Min and Clothiaux, 2003; Min and Harrison, 2004; Min et al., 2004c; Li and Min, 2008). With current resolving power of HABS, however, four or five independent pieces of information can be retrieved from the measured spectra. It is advantageous to combine HABS with other sensors, in particular, with active lidar and radar systems. For example, cloud radar signal is capable of penetrating clouds and revealing multiple layers aloft. However, the observed radar reflectivity is a function of the sixth moment of the hydrometeor particle size distribution. It requires an assumption of particle size distribution to retrieve cloud water content (the third moment of the hydrometeor particle size distribution) for practical applications from radar reflectivity. As the pressure dependence of oxygen A-band

AMTD
7, 1027–1057, 2014

absorption line parameters provides vertical resolving power and photon path length information inferred from oxygen A-band spectra is a function of the second moment of particle size distribution, HABS measured oxygen A-band spectra can be used to better constrain the assumed particle size distribution of radar retrievals, particularly for multi-layer clouds and for mixed-phase clouds (Li and Min, 2013). With the polarization capability of HABS, combining of HABS observations with lidar measurements provides better retrievals of vertical profiles of aerosols and thin clouds. We will explore those capabilities in the near future.

Acknowledgements. This work was supported by US DOE's Atmospheric System Research program (Office of Science, OBER) under contract DE-FG02-03ER63531, by the NSF under contract AGS-1138495, and by the NOAA Educational Partnership Program with Minority Serving Institutions (EPP/MSI) under cooperative agreements NA17AE1625 and NA17AE1623. Part of this research was also supported by Strategic Priority Research Program of the Chinese Academy of Sciences (XDA05040300) and National High Technology Research and Development Program of China (No.2011AA12A104).

References

Berry, H. G, Gabrielse, G., and Livingston, A. E.: Measurement of the stokes parameters of light, Appl. Optics, 16, 3200–3205, doi:10.1364/AO.16.003200, 1997.

Chou, M. D. and Kouvaris, L.: Monochromatic calculation of atmospheric radiative transfer due to molecular line absorption, J. Geophys. Res., 91, 4047–4055, 1986.

Chowdhary, J., Cairns, B., Mishchenko, M., and Travis, L.: Retrieval of aerosol properties over the ocean using multispectral and multiangle photopolarimetric measurements from the Research Scanning Polarimeter, Geophys. Res. Lett., 28, 243–246, 2001.

Chowdhary, J., Cairns, B. Mishchenko, M. I., Hobbs, P. V., Cota, G. F., Redemann, J., Rutledge, K., Holben, B. N., and Russell, E.: Retrieval of aerosol scattering and absorption properties from photopolarimetric observations over the ocean during the CLAMS experiment, J. Atmos. Sci., 62, 1093–1117, 2005.

AMTD
7, 1027–1057, 2014

Clough, S. A., Shephard, M. W., Mlawer, E. J., Delamere, J. S., Iacono, M. J., Cady-Pereira, K., Boukabara, S., and Brown, P. D.: Atmospheric radiative transfer modeling: a summary of the AER codes, J. Quant. Spectrosc. Ra., 91, 233–244, 2005.

Connell, R. M., Adam, M., and Venable, D.: A numerical model of the performance of the Howard University Raman Lidar System, AIP Conf. Proc., 1140, 99–103, doi:10.1063/1.3183533, 2009.

Duan, M., Min, Q., and Li, J.: A fast radiative transfer model for simulating high-resolution absorption bands, J. Geophys. Res., 110, D15201, doi:10.1029/2004JD005590, 2005.

Fischer, J. and Grassl, H.: Detection of cloud-top height from backscattered radiances within the oxygen A band. Part I: Theoretical study, J. Appl. Meteorol., 30, 1245–1259, 1991.

Fischer, J., Cordes, W., Schmitz-Peiffer, A., Renger, W., and Morel, P.: Detection of cloud-top height from backscattered radiances within the oxygen A band. Part II: Measurements, J. Appl. Meteorol., 30, 1260–1267, 1991.

Grechko, Y. I., Dianov-Klokov, V. I., and Malkov, I. P.: Aircraft measurements of photon paths in reflection and transmission of light by clouds in the 0.76 um oxygen band, Atmos. Ocean. Phys., 9, 471–485, 1973.

Harrison, L. and Min, Q.-L.: Photon pathlength distributions in cloudy atmospheres from ground-based high-resolution O_2 A-band spectroscopy, in: IRS'96: Current Problems in Atmospheric Radiation, edited by: Smith, W. L. and Stamnes, K., Deepak Pub, Hampton, 594–602, 1997.

Heidinger, A. and Stephens, G. L.: Molecular line absorption in a scattering atmosphere, 2: Retrieval of particle properties, J. Atmos. Sci., 57, 1615–1634, 2000.

Heidinger, A. and Stephens, G. L.: Molecular line absorption in a scattering atmosphere, 3: Path length characteristics and effects of spatially heterogeneous clouds, J. Atmos. Sci., 59, 1641–1654, 2002.

Lacis, A. A., Chowdhary, J., Mishchenko, M. I., and Cairns, B.: Modeling errors in diffuse-sky radiation: vector versus scalar treatment, J. Geophys. Res., 25, 135–138, 1998.

Levy, R. C., Remer, L. A., and Kaufman, Y. J.: Effects of neglecting polarization on the MODIS aerosol retrieval over land, IEEE T. Geosci. Remote, 42, 2576–2583, 2004.

Li, S. and Min, Q.: Diagnosis of multilayer clouds using photon path length distributions, J. Geophys. Res., 115, D20202, doi:10.1029/2009JD013774, 2010.

Li, S. and Min, Q.: Wavelength registration of high resolution oxygen A-band spectral measurements, J. Quant. Spectrosc. Ra., 122, 106–123, doi:10.1016/j.jqsrt.2012.10.024, 2012.

AMTD
7, 1027–1057, 2014

Li, S. and Min, Q.: Retrievals of vertical profiles of stratus cloud properties from combined oxygen A-band and radar observations, J. Geophys. Res.-Atmos., 118, 769–778, doi:10.1029/2012JD018282, 2013.
McMaster, W. H.: Polarization and the Stokes Parameters, Am. J. Phys., 22, 351, doi:10.1119/1.1933744, 1954.
McMaster, W. H.: Matrix representation of polarization, Rev. Mod. Phys., 33, 8–28, doi:10.1103/RevModPhys.33.8, 1961.
Min, Q.-L. and Clothiaux, E. E.: Photon path length distributions inferred from rotating shadowband spectrometer measurements at the Atmospheric Radiation Measurements Program Southern Great Plains site, J. Geophys. Res., 108, D154465, doi:10.1029/2002JD002963, 2003.
Min, Q.-L. and Duan, M.: A successive order of scattering model for solving vector radiative transfer in the atmosphere, J. Quant. Spectrosc. Ra., 87, 243–259, 2004.
Min, Q.-L. and Harrison, L. C.: Cloud properties derived from surface MFRSR measurements and comparison with GOES results at the ARM SGP site, Geophys. Res. Lett., 23, 1641–1644, 1996.
Min, Q.-L. and Harrison, L. C.: Joint statistics of photon path length and cloud optical depth, Geophys. Res. Lett., 26, 1425–1428, 1999.
Min, Q.-L. and Harrison, L. C.: Retrieval of atmospheric optical depth profiles from downward-looking high-resolution O_2 A-band measurements: optically thin conditions, J. Atmos. Sci., 61, 2469–2478, 2004.
Min, Q.-L., Harrison, L. C., and Clothiaux, E.: Joint statistics of photon pathlength and cloud optical depth: case studies, J. Geophys. Res., 106, 7375–7386, 2001.
Min, Q.-L., Duan, M., and Marchand, R.: Validation of surface retrieved cloud optical properties with in situ measurements at the Atmospheric Radiation Measurement Program (ARM) South Great Plains site, J. Geophys. Res., 108, D174547, doi:10.1029/2003JD003385, 2003.
Min, Q.-L., Joseph, E., and Duan, M.: Retrievals of thin cloud optical depth from a multifilter rotating shadowband radiometer, J. Geophys. Res., 109, D02201, doi:10.1029/2003JD003964, 2004a.
Min, Q.-L., Minnis, P., and Khaiyer, M.: Comparison of cirrus optical depths derived from GOES 8 and surface measurements, J. Geophys. Res., 109, D15207, doi:10.1029/2003JD004390, 2004b.

AMTD
7, 1027–1057, 2014

Min, Q.-L., Harrison, L. C., Kierdron, P., Berndt, J., and Joseph, E.: A high-resolution oxygen A-band and water vapor band spectrometer, J. Geophys. Res., 109, D02202, doi:10.1029/2003JD003540, 2004c.

Min, Q., Wang, T., Long, C. N., and Duan, M.: Estimating fractional sky cover from spectral measurements, J. Geophys. Res., 113, D20208, doi:10.1029/2008JD010278, 2008.

Mishchenko, M. I., Lacis, A. A., and Travis, L. D.: Errors induced by the neglect of polarization in radiance calculations for Rayleigh-scattering atmospheres, J. Quant. Spectrosc. Ra., 51, 491–510, 1994.

Mitchell, R. M. and O'Brien, D. M.: Error estimates for passive satellite measurement of surface pressure using absorption in the A band of oxygen, J. Atmos. Sci., 44, 1981–1990, 1987.

Natraj, V., Spurr, R., Boesch, H., Jiang, Y., and Yung, Y.: Evaluation of errors in neglecting polarization in the forward modeling of O_2 A band measurements from space, with relevance to CO_2 column retrieval from polarization sensitive instruments, J. Quant. Spectrosc. Ra., 103, 245–259, 2007.

O'Brien, D. M. and Mitchell, R. M.: Error estimates for retrieval of cloud top pressure using absorption in the A band of oxygen, J. Appl. Meteorol., 31, 1179–1192, 1992.

Oikarinen, L.: Polarization of light in UV-visible limb radiance measurements, J. Geophys. Res., 106, 1533–1544, 2001.

Pfeilsticker, K., Erle, F., Veitel, H., and Platt, U.: First geometrical pathlengths probability density function derivation of the skylight from spectroscopically highly resolving oxygen A-band observations: 1. Measurement technique, atmospheric observations and model calculations, J. Geophys. Res., 103, 11483–11504, 1998.

Portmann, R. W., Solomon, S., Sanders, R. W., and Danel, J. S.: Cloud modulation of zenith sky oxygen path lengths over Boulder, Colorado: measurements versus model, J. Geophys. Res., 106, 1139–1155, 2001.

Rothman, L. S., Gordon, I. E., Barbe, A., Benner, D. C., Bernath, P. F., Birk, M., Boudon, V., Brown, L. R., Campargue, A., Champion, J.-P., Chance, K., Coudert, L. H., Dana, V., Devi, V. M., Fally, S., Flaud, J.-M., Gamache, R. R., Goldman, A., Jacquemart, D., Kleiner, I., Lacome, N., Lafferty, W. J., Mandin, J.-Y., Massie, S. T., Mikhailenko, S. N., Miller, C. E., Moazzen-Ahmadi, N., Naumenko, O. V., Nikitin, A. V., Orphal, J., Perevalov, V. I., Perrin, A., Predoi-Cross, A., Rinsland, C. P., Rotger, M., Simeckova, M., Smith, M. A. H., Sung, K., Tashkun, S. A., Tennyson, J., Toth, R. A., Vandaele, A. C., and Auwera, J. V.: The HITRAN 2008 molecular spectroscopic database, J. Quant. Spectrosc. Ra., 110, 533–572, 2009.

AMTD
7, 1027–1057, 2014

Schutgens, N. A. J. and Stammes, P.: A novel approach to the polarization correction of space-borne spectrometers, J. Geophys. Res., 108, D74229, doi:10.1029/2002JD002736, 2003.
Stam, D. M. and Hovenier, J. W.: Errors in calculated planetary phase functions and albedos due to neglecting polarization, Astron. Astrophys., 444, 275–286, 2005.
Stamnes, K., Tsay, S. C., Jayaweera, K., and Wiscombe, W.: Numerically stable algorithm for discrete ordinate method radiative transfer in multiple scattering and emitting layered media, Appl. Optics, 27, 2502–2509, 1988.
Stephens, G. L. and Heidinger, A.: Molecular line absorption in a scattering atmosphere: I Theory, J. Atmos. Sci., 57, 1599–1614, 2000.
Stephens, G. L., Heidinger, A., and Gabriel, P.: Photon paths and cloud heterogeneity: toward an observational strategy for assessing the effects of 3D geometry on radiative transfer, Three-Dimensional Radiative Transfer for Cloudy Atmospheres, 2005.
Veitel, H., Funk, O., Kruz, C., Platt, U., and Pfeilsticker, K.: Geometrical pathlength probability density functions of the skylight transmitted by midlatitude cloudy skies: some case studies, Geophys. Res. Lett., 25, 3355–3358, 1998.

AMTD
7, 1027–1057, 2014

Fig. 1. The photo of the HABS taken at the Atmospheric Science and Research Center, State University of New York at Albany during the field observation.

AMTD
7, 1027–1057, 2014

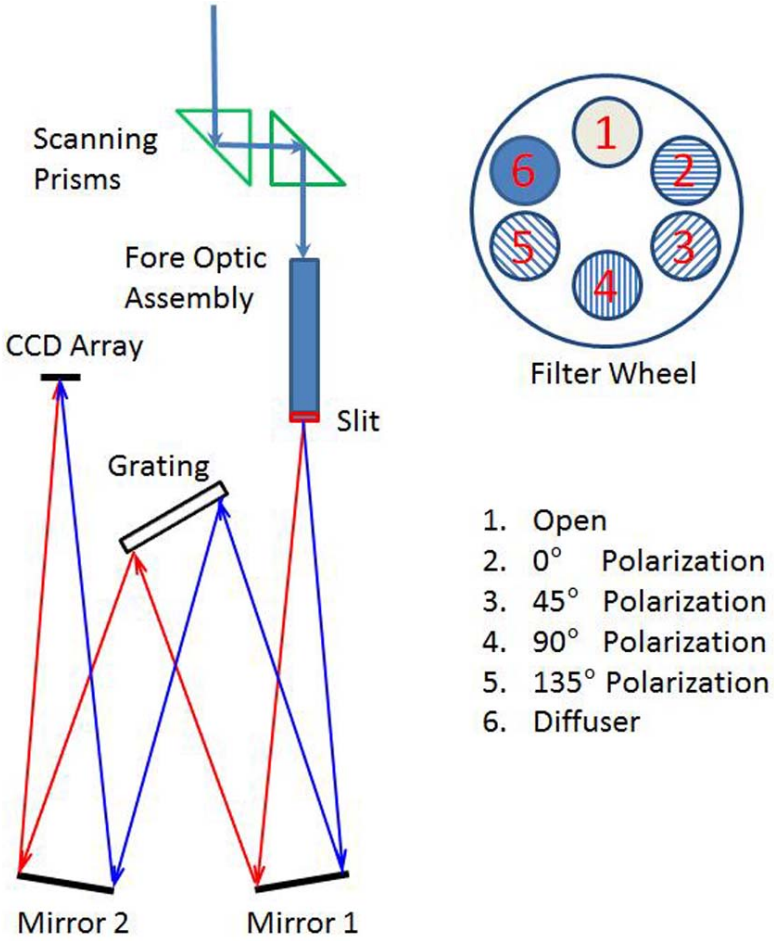

Fig. 2. The schematic of the high-resolution oxygen A-band spectrometer (HABS) optical system.

AMTD
7, 1027–1057, 2014

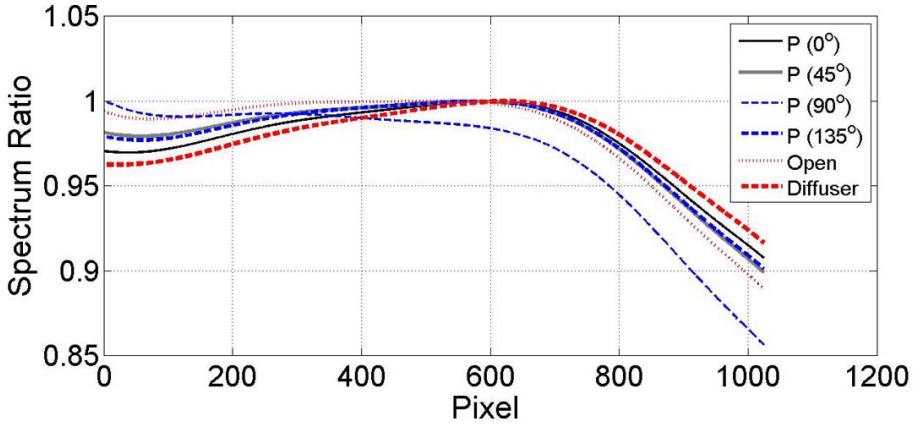

Fig. 3. Spectrum response ratios to the lamp GS0937 at different channels (i.e., open, diffuser, and 4 polarizers with different orientations) of the filter wheel.

AMTD
7, 1027–1057, 2014

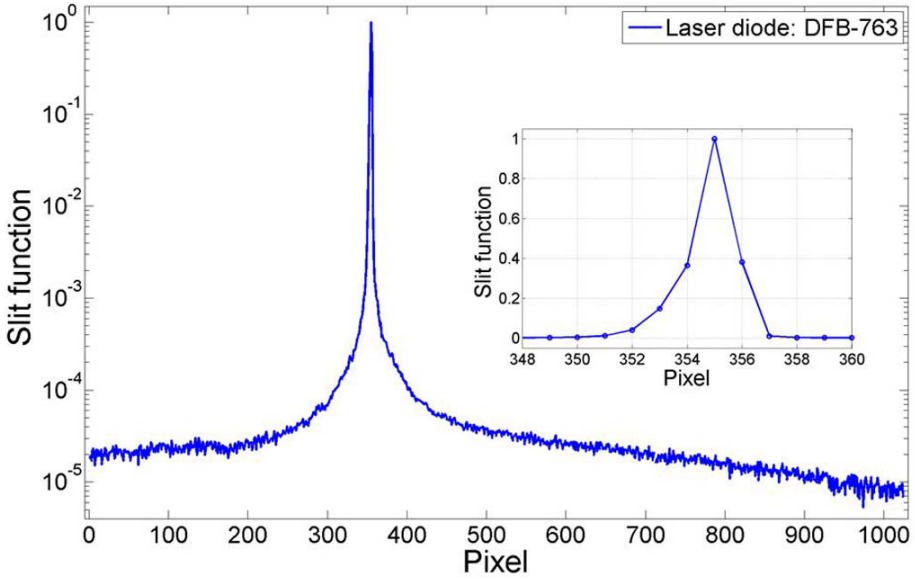

Fig. 4. Slit function of high-resolution oxygen A-band spectrometer (HABS) with a 1.55 pixels FWHM. The inner figure is an expansion of the slit function in linear scale.

AMTD
7, 1027–1057, 2014

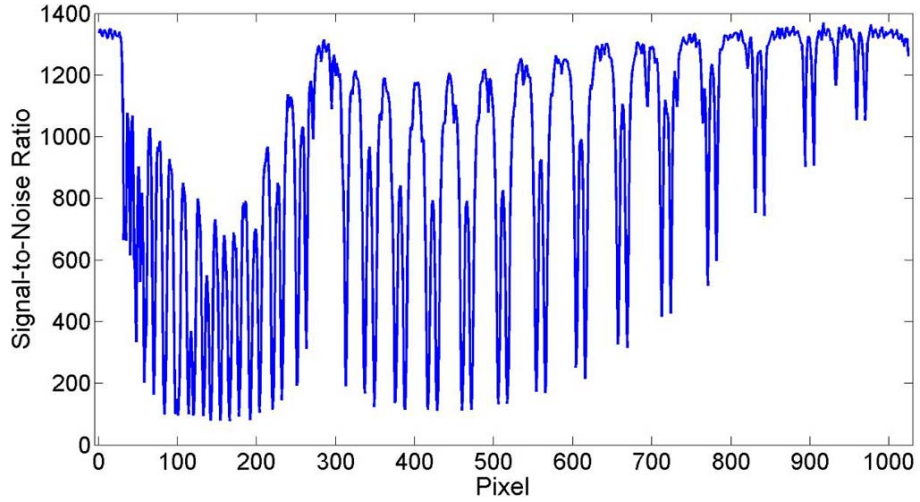

Fig. 5. Estimated signal-to-noise ratio (SNR) at 19:13 (GMT) on 14 June 2011 at Howard University Beltsville site.

AMTD
7, 1027–1057, 2014

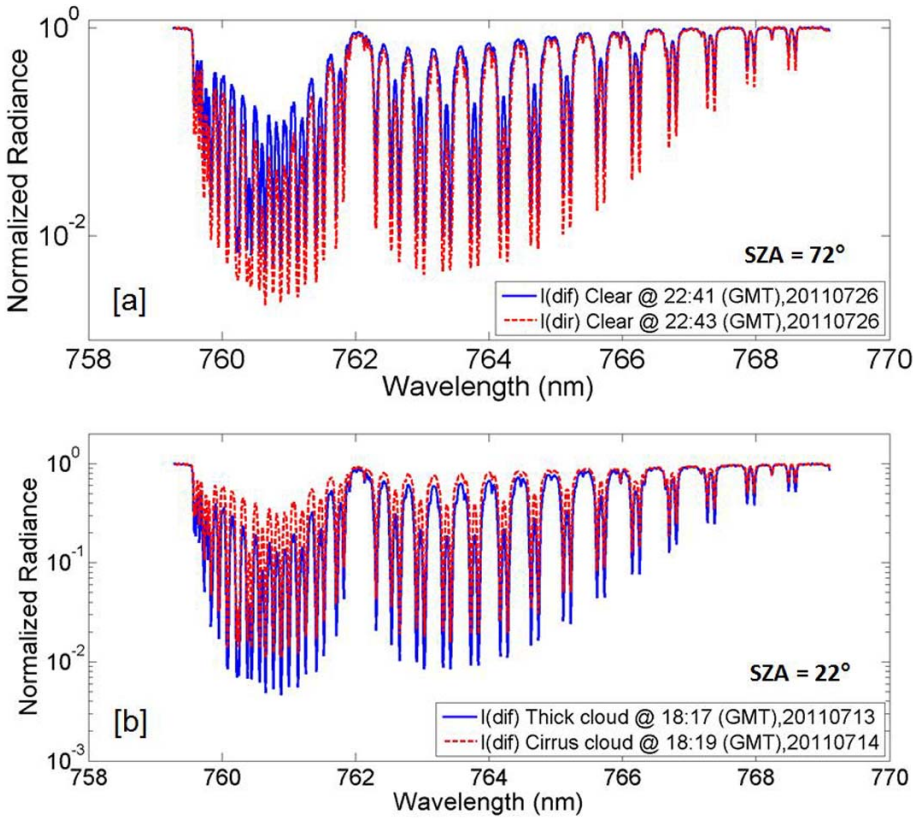

Fig. 6. (a) HABS measured direct beam spectra and zenith diffuse spectra at oxygen A-band under clear day situations at solar zenith angle of 72°. **(b)** Two HABS measured zenith diffuse spectra at oxygen A-band under different cloudy situations at solar zenith angle of 22°.

AMTD
7, 1027–1057, 2014

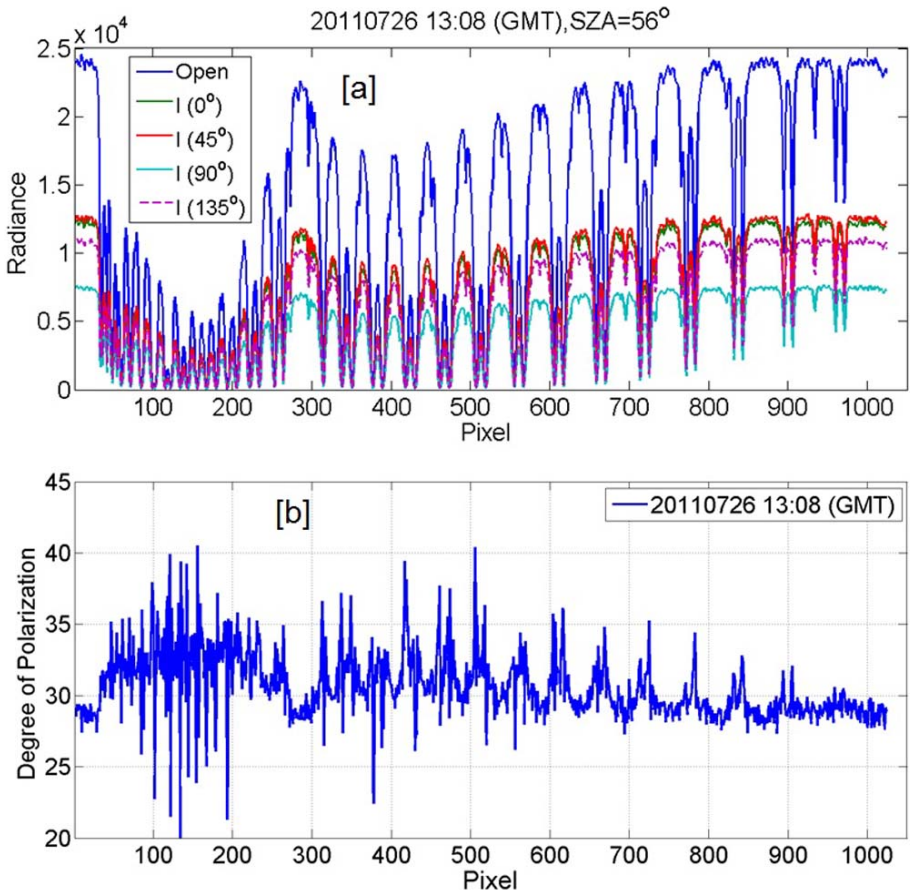

Fig. 7. (a) Measured high-resolution oxygen A-band spectra of diffuse radiation at the zenith direction and **(b)** the related derived degree of polarization (DOP) spectrum at 13:08 (GMT) on 26 July 2011. The radiance is indicated by the Analog to Digital Converter (ADC) counts.

AMTD
7, 1027–1057, 2014

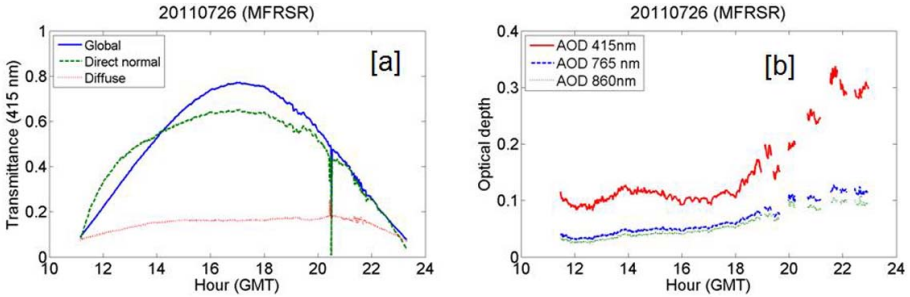

Fig. 8. (a) Daily variation of direct normal, global horizontal and diffuse horizontal irradiances from MFRSR measurements on 26 July 2011 at Howard University Beltsville site. **(b)** Daily variation of derived aerosol optical depth at 415, 760 and 870 nm from MFRSR measurements.

AMTD
7, 1027–1057, 2014

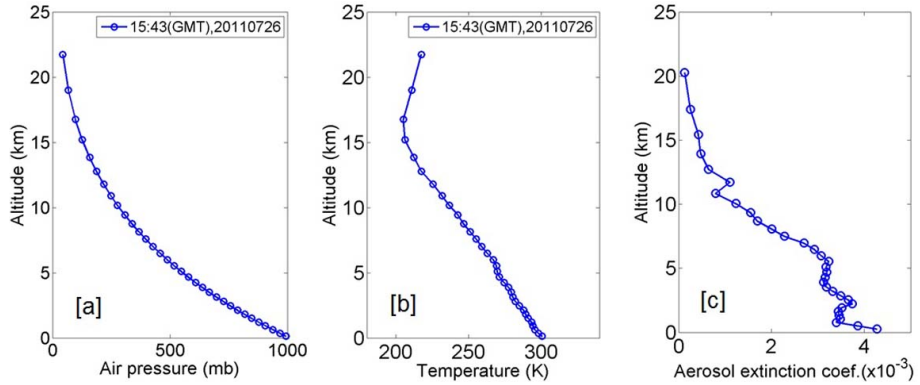

Fig. 9. Profiles of **(a)** air pressure and **(b)** temperature from sonde balloon measurements at 15:43 (GMT) on 26 July 2011 at Howard University Beltsville site. **(c)** Aerosol extinction coefficients profile estimated from Raman Lidar measured aerosol scattering ratio profile coupled with MFRSR derived AOD.

AMTD
7, 1027–1057, 2014

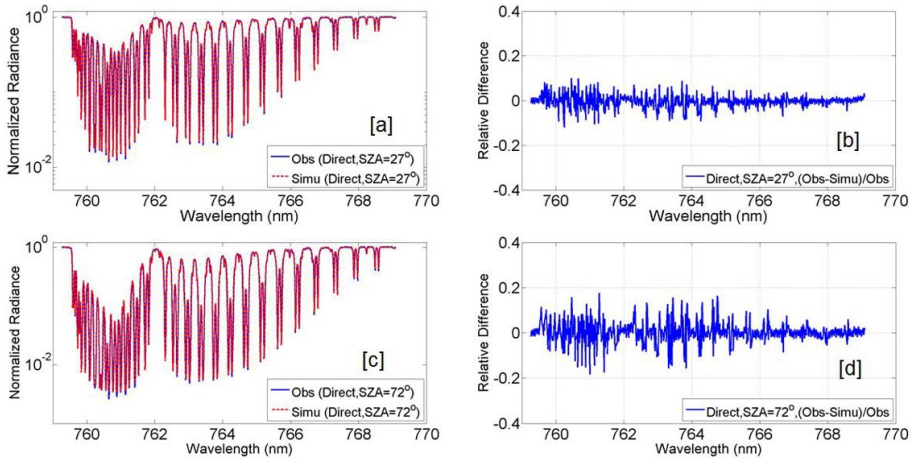

Fig. 10. Comparisons of normalized radiance of HABS measured and model simulated direct-beam spectra at oxygen A-band under different solar zenith angles.

AMTD
7, 1027–1057, 2014

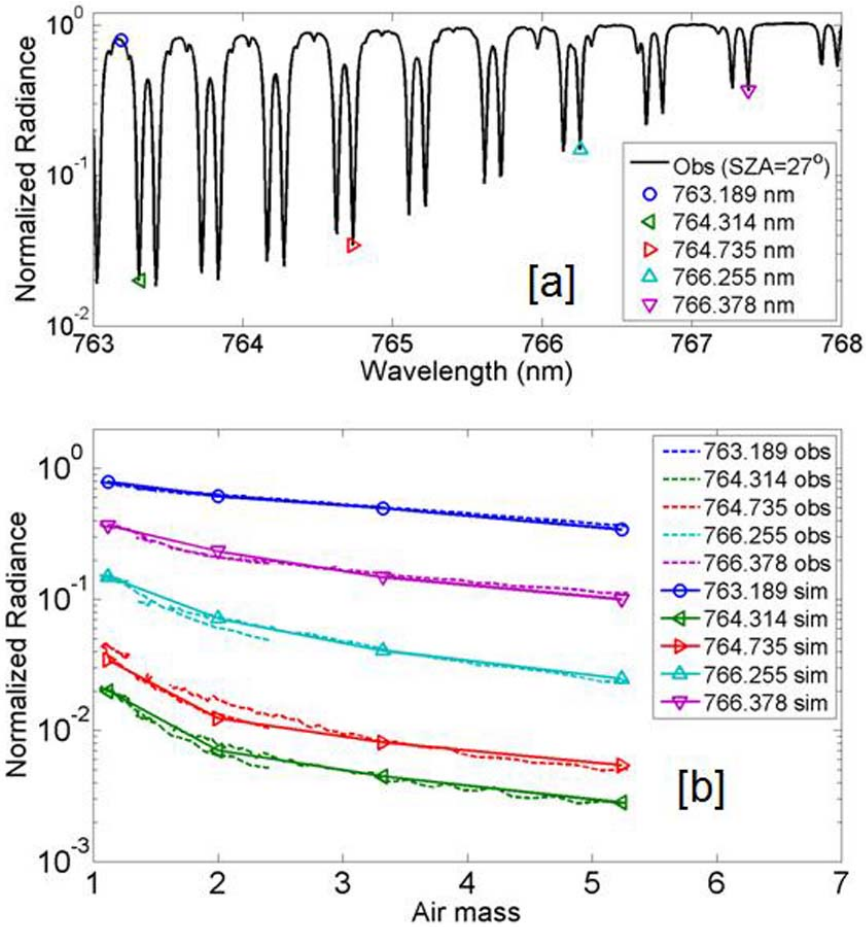

Fig. 11. Comparisons of normalized radiance of HABS measured and model simulated direct-beam spectra at oxygen A-band vs. air mass.

AMTD
7, 1027–1057, 2014

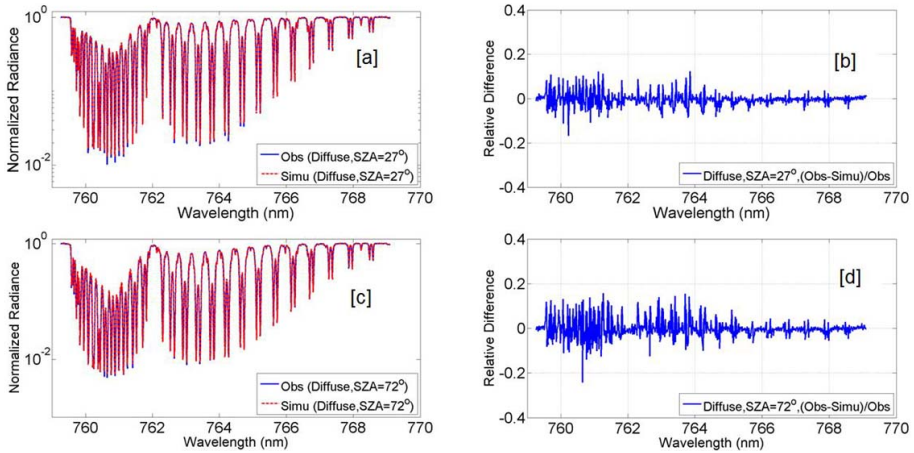

Fig. 12. Comparisons of measured and simulated diffuse spectra at oxygen A-band for solar zenith angles of 27° (**a** and **b**) and 72° (**c** and **d**).

AMTD
7, 1027–1057, 2014